

Relationship Between Structure and Solubility of Thiol-Protected Silver Nanoparticles and Assemblies

Christina A. Bauer · Francesco Stellacci ·
Joseph W. Perry

Published online: 29 February 2008
© Springer Science+Business Media, LLC 2008

Abstract The solubility of alkythiol-coated silver nanoparticles and the energetics of the ligand disordering have been investigated. Calorimetry measurements have provided correlations between the nature of the ligands and the enthalpy of the ligand disordering, which have guided the improvement of nanoparticle solubility and dispersion in organic media.

Keywords Metal nanoparticles · Silver nanoparticles · Ligand-coated nanoparticles · Order-disorder transition · Nanoparticle solubility · Nanoparticle assemblies

1 Introduction

Metal nanoparticles are responsible for the coloration of many glass objects that can be dated back at least to ancient Roman times, as well as of medieval stained glass windows. However, their elemental composition and role as colorant was not established until Faraday carried out his groundbreaking work in 1857, wherein he concluded that

the intense red color of certain stained glass derived from small particles of gold [1]. He described a relatively simple process for making colloidal suspensions of gold nanoparticles in water that were stable over time. Although nanoparticles of metals, metal oxides, and other materials differ in their properties, they all require stabilization from aggregation to avoid formation of the thermodynamically more stable bulk materials.

A significant breakthrough in the synthesis of metal nanoparticles occurred in 1994, when Brust took advantage of the known self-assembly of thiols on gold surfaces to create charge-neutral gold nanoparticles coated with alkythiols [2]. Two general solution-based synthetic strategies have been reported: one that utilizes a phase-transfer agent and an alternative homogeneous route reported subsequently [3]. These broadly applicable synthetic schemes, commonly termed ‘two-phase’ and ‘one-phase’, respectively, produce particles that are “passivated” with surface bound ligands that provide improved long-term stability. Both syntheses yield metal nanoparticles that can be produced in and, isolated and stored under ambient conditions as a free-flowing powder for later dissolution, which allows them to be handled and derivatized in manners familiar to synthetic chemists. Further modification of gold nanoparticles via functionalization of the ω -terminal group of the ligand and/or place exchange reactions has been demonstrated [4]. Following the intense interest generated by the facile synthesis of “stable” and soluble gold nanoparticles, similar preparations of silver nanoparticles coated with alkythiols began to appear in the literature [5].

The ligand molecules adsorbed on gold and silver nanoparticles perform multiple functions. They serve to cap the nanocrystals during growth at a particular size and to protect them from further aggregation. However, the

C. A. Bauer · F. Stellacci
Department of Chemistry, University of Arizona,
1306 E. University Blvd., Tucson, AZ 85721-0041, USA

C. A. Bauer · J. W. Perry (✉)
School of Chemistry and Biochemistry, Georgia Institute
of Technology, 901 Atlantic Drive NW, Atlanta,
GA 30332-0400, USA
e-mail: joe.perry@gatech.edu

Present Address:
F. Stellacci
Department of Materials Science and Engineering,
Massachusetts Institute of Technology, 77 Massachusetts Ave.,
Cambridge, MA 02139, USA

ligands that are commonly utilized to impart solubility can also lead to interdigitation with those on neighboring particles, leading to strong cohesive interactions between nanoparticles to form tightly-packed particle assemblies [6]. Although this phenomenon is useful for preparing close-packed, ordered assemblies [7], it can also result in unwanted aggregation and phase separation in solutions and polymer matrices. A variety of experiments have shown that when condensed into films, the ligand shells of neighboring particles tend to interact in a space-filling manner. Chain–chain interactions can arise from densely packed domains on a single particle or by interdigitation of chain domains between neighboring particles. TEM images of alkylthiol coated gold particles reveal that the interparticle spacing approaches the distance of one all-*trans* ligand length, supporting the notion of some form of interdigitation of the ligands [8, 9]. The ligand ordering can be probed by differential scanning calorimetry (DSC) and IR spectroscopy, which have supported that alkyl chains of five or more carbons are in an extended, mostly *trans* state [10]. Interdigitation and bundling of thiolates between neighboring silver nanoparticles has been imaged with energy filtered TEM [11]. The attractive interactions associated with ligand interdigitation provides a strong driving force for aggregation of metal nanoparticles and can lead to phase segregation of dispersions of nanoparticles in polymer hosts.

The recent advances in metal nanoparticle synthesis have opened the door to many potential applications. Metallic nanoparticles in particular have been exploited in applications in catalysis [12], electronics [13], and surface-enhanced spectroscopies [14] to name but a few. Examples of applications of polymer-nanoparticle composites include metallodielectric photonic crystals based on diblock copolymers [15], oriented arrays of nanoparticles in polymers to form polarization-dependent color filters [16], and laser 3-D metal writing in polymer films [17]. In order to effectively utilize these particles in applications, it is vital that both the structures and properties of individual nanoparticles and their assemblies are understood. In particular, the processibility of metal nanoparticles is an extremely important factor for the manufacturing of reproducible composites and devices.

Although gold and silver nanoparticles share a structural similarity in that they both consist of a polarizable core, surrounded by a shell of ligands that extend radially outward from the core [18], they also can be expected to exhibit unique structural characteristics, owing to the differences in metal-thiolate bonding. For instance, in our studies, we have noted significant differences in solubility between these two metals, where silver nanoparticles generally show more limited solubility. In the laser writing in metal nanoparticle composites [17], Stellacci et al.

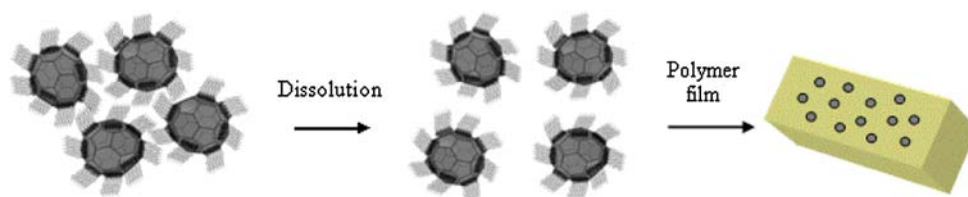
found that enhancement of nanoparticle solubility was crucial to successfully implement the process. It is clear that understanding of the structure-property relationships of alkylthiol ligands on nanoparticles is an important element in successfully tailoring superstructures and composites of ligand coated nanoparticles.

In this paper, we report on a study of the energetics of the order-disorder transition of alkylthiol coated silver nanoparticles, for different alkyl chain lengths, mean core diameter of the particles, and ligand coatings comprised of mixtures of different ligands. The calorimetry data for a selection of nanoparticles was correlated to their solubility and the structure-properties trends that emerge allow for qualitative and quantitative prediction of nanoparticle solubility. This manuscript is organized as follows: We begin with a discussion of the synthesis and characterization of the alkylthiol nanoparticles studied. The results of DSC measurements on quasi-ordered solids of alkylthiol coated silver nanoparticles are then presented and the thermodynamic properties of the order-disorder transition are discussed. The role of polyfunctionalization through use of ligand mixtures and terminal substitutions for improvement of nanoparticle dispersion in polymer hosts are highlighted. We present the solubility of a selection of nanoparticles and the correlation with the disordering energetics. We also present an analysis of material isolated directly from the synthesis, and corresponding soluble and insoluble fractions isolated therefrom.

2 Results and Discussion

Figure 1 shows an illustration of particle interdigitation and the dissolution process, followed by incorporation into a polymer film as discrete, non-aggregated particles. We have investigated several ways of reducing the extent of interdigitation of the ligand chains in order to enhance the solubility of the particles. To this end, a series of silver nanoparticles was synthesized, wherein the alkylthiol ligand chain length and silver core size were varied, multiple ligands were attached to the particles, and ligands bearing carbazole terminal groups, that promote favorable interaction with a polyvinylcarbazole (PVK) matrix, were added. With a thorough understanding of the ordering of the alkyl chains and the factors that govern this, a reasonable series of alterations can be expected to increase disorder and hence increase solubility. The common, two-phase synthesis of metallic nanoparticles is versatile, but one major drawback is the difficulty in removing the phase transfer agent (typically tetraoctylammonium bromide, TOAB) and (in the case of gold) disulfides, which are byproducts from the reduction of gold (III) to gold (I). A comparison between silver nanoparticles prepared in a one- and two-phase method has been reported [19]. Through a

Fig. 1 Schematic illustration of an interdigitated assembly of metal nanoparticles, dissolution in solvent resulting in dissociation of the assembly, and formation of a polymer-nanocomposite film



variety of methods, including IR and TEM, it was shown that the two types of particles were essentially the same, although those produced in the one-phase synthesis displayed more alkyl chain order in the ligand shell. This is most likely a result of contamination by TOAB in the two-phase synthesis, which remains a topic of current concern [20]. Despite these advantages, the one-phase method remains less prevalent in the literature [21].

We utilized the one-phase method to prepare a series of *n*-alkylthiol-coated silver nanoparticles to systematically explore the effects of structure on the disordering enthalpy and solubility. It is well known that the particle size can be adjusted by altering the silver to thiol ratio [22]. Other degrees of freedom for modifying the particle composition include changes in ligand length and polyfunctionalization [23] with more than one ligand in particular ratios. The characterization of nanoparticles polyfunctionalized with *n*-alkylthiols is discussed below. A summary of the control of core size with alteration of silver/thiol ratios are shown for a variety of ligands in Table 1. It can be seen that in both the mixed and monoligand cases, the size is directly related to the silver/ligand molar ratios. It is also interesting to note that a mixture of octylthiol and dodecylthiol in the nanoparticle shell results in consistently larger particles

Table 1 Characterization of silver nanoparticle composition and size by elemental analysis and TEM

Ligand(s)	$n_{\text{Ag}}/n_{\text{thiol}}$ feed ratio	$n_{\text{Ag}}/n_{\text{thiol}}$ determined for final particle	Particle size (nm)
Octylthiol/ Dodecylthiol	3.0	3.4	10.1 ± 2.0
Octylthiol/ Dodecylthiol	1.5	1.7	4.9 ± 1.6
Octylthiol	1.2	1.6	2.0 ± 0.6
Octylthiol	3.0	3.9	4.0 ± 1.0
Octylthiol	9.0	6.6	9.7 ± 1.9
Hexylthiol	6.0	7.5	5.9 ± 1.8
Hexylthiol	3.0	5.8	3.1 ± 0.6

The ligand(s) used are shown in the first column, the silver to thiol molar ratios used in synthesis (feed ratio) in the second column, and the metal to thiol ratio determined for the particles by elemental analysis in the third. The fourth column shows the average particle size as determined by TEM. The octylthiol/dodecylthiol molar ratio for the first two samples was 1:1

than for the nanoparticles with monoligand shells. This may indicate that the disorder induced by ligand mixtures results in a smaller degree of core passivation and the formation of larger nanoparticles during the growth.

Our synthesis of mixed-ligand nanoparticles involves simple addition of two (or more) ligands in the desired ratio in the first step of the reaction. A variety of experiments were performed to determine if polyfunctionalization of silver nanoparticles is possible in a controlled manner. To begin with, the relative ratios of the different *n*-alkylthiols present on the surface of the synthesized nanoparticles were determined. In this experiment, iodine was added to the nanoparticles in dichloromethane, which led to the precipitation of AgI and the oxidation of the alkylthiolates to alkyldisulfides [4b]. Three separate mass peaks were detected by gas chromatography/mass spectrometry (which correspond to the three possible disulfide combinations for nanoparticles coated with a binary mixture of ligands), the relative intensities of which revealed the relative ratio of these thiols on the particles. These were determined to agree, within experimental error, with the ratio of thiols added initially. It is probable that these disulfides derive from mixed-ligand nanoparticles as opposed to a mixture of two homogeneously-coated ligand-stabilized silver nanoparticles, especially when considering the lability of the silver-thiolate bond [24]. To confirm this, DSC measurements were conducted where it was observed that a mixture of two different types of nanoparticles, each with a different ligand, can be annealed via a series of heating cycles to form mixed-ligand nanoparticles by rapid ligand exchange. These experiments are discussed in greater detail below.

DSC has proven to be one of the most useful tools for characterizing nanoparticle assemblies in the work presented here. When coupled with optical microscopy, powder X-ray diffraction (XRD) and IR spectroscopy, DSC can be very powerful in the understanding of the thermodynamics of nanoparticle assemblies. Previously, DSC has been used for identifying phase transitions in ligand-coated gold nanoparticles. Briefly, gold nanoparticles in the solid phase undergo a disordering process [8]. The bulk solid material is not found to melt after this transition occurs; in conjunction with temperature-controlled IR, the disordering process has been assigned to the melting of the alkylthiol chains surrounding the nanoparticle cores. Both

the enthalpy change and temperature of these disordering events are strongly dependent on the length of the alkylthiols present, and the phase transitions are nearly undetectable for gold nanoparticles coated with ligands shorter than dodecylthiol. The chain melting of n - C_nH_{2n+1} thiol-coated gold nanoparticles occurs at the following temperatures for the indicated chain length: 3 °C ($n = 12$), 22 °C ($n = 14$), 41 °C ($n = 16$), 51 °C ($n = 18$), and 64 °C ($n = 20$) [25]. These ‘melting’ transition temperatures are quite comparable to those found for gold SAMs, for which the temperatures are found to be: 39 °C ($n = 16$), 53 °C ($n = 18$), and 63 °C ($n = 20$), measured electrochemically [26]. Gold nanoparticles coated with alkylthiol chains having 12, 10, and 8 carbons display broad melt transitions at temperatures less than 0 °C, indicating they are melted at room temperature, as evidenced by the viscous nature of these materials. However, IR studies reveal that although nanoparticles protected with these shorter ligands are macroscopically melted, they are in a microcrystalline ordered state [10]. The transitions for gold nanoparticles are very broad, occurring across a range of some 30 °C, which is considerably broader than the 5 °C ranges that have been determined for typical gel-to-liquid crystalline transitions observed for lipid bilayer membranes [9].

We found that upon preparation of silver nanoparticles by the one-phase method, a portion of the product is soluble in organic solvents, and a fraction is not. Initial studies discussed here were conducted on the raw, as-prepared nanoparticles. Further studies on the ‘purified’ particles, wherein the soluble portion was separated from the insoluble portion, will be discussed below. Thermogravimetric analysis (TGA) showed that mass loss for the silver nanoparticles studied does not occur before 250 °C, so DSC measurements were performed by cycling the temperature from 20 °C to 220 °C. First, monofunctionalized particles of various sizes were studied; see Fig. 2 for illustrative DSC scans of octylthiol-coated nanoparticles.

There is a large amount of information to be drawn from the DSC traces and this will be summarized here. A sharp reversible transition is evident at 127 °C (increasing temperature scan). This peak is fully reversible, where the reverse process occurs at 112 °C, at the scan speed used, and appears at slightly lower temperature in the second cycle. This is followed by an irreversible transition at high temperatures (180–200 °C), which is seen for all nanoparticle samples studied. This is assigned to a degradative process without mass loss. Additionally, there is a peak of relatively small enthalpy that is observed for the nanoparticles with the octyl ligand at approximately 63 °C (Fig. 2b); this peak is also reversible and often gains in sharpness after a second cycle, most likely a result of annealing of the ligand shell. These low temperature transitions are only observed for ligands where $n < 12$, likely due to a lesser degree of order in the cases with shorter chain ligands, as summarized in Table 2.

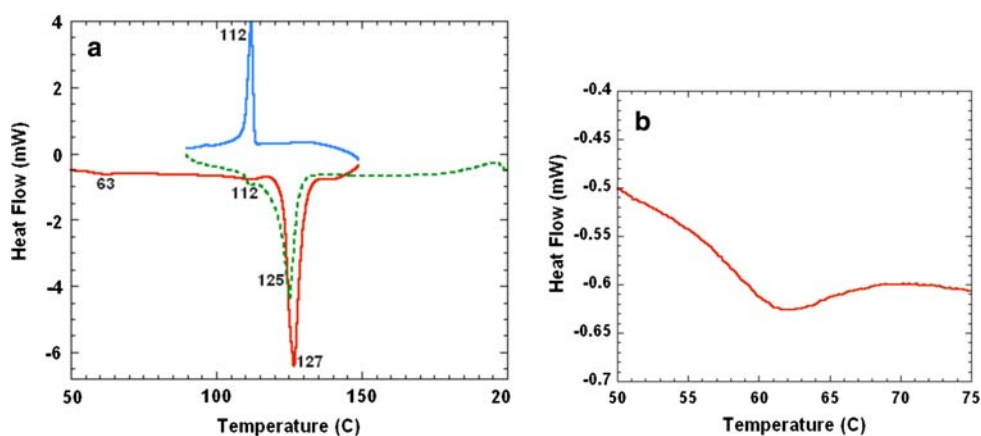
In contrast to gold nanoparticles, silver nanoparticles coated with alkylthiols of different lengths containing an even number of carbons in the chain exhibit this phase transition at nearly the same temperature. However, the energetics of the transitions differ, steadily decreasing with a decrease in ligand length. The high temperature of the

Table 2 Transition temperatures of the lowest temperature peak for alkylthiol-coated silver nanoparticles with $n = 6$ –11

Sample number	Ligand chain length	Transition temperature (°C)
3	C ₉	64
4	C ₈	67
11	C ₈	63
5	C ₇	85
6	C ₆	74

Temperature variations are ± 2 °C for various core sizes. Refer to Table 3 for sample numbers and identities

Fig. 2 DSC of octylthiol-coated silver nanoparticles prepared with a 3:1 metal to ligand ratio (peaks pointing down are endothermic). (a) The first heating scan is shown in red, the reverse in blue, and the second heating in dotted green. (b) The low temperature endothermic peak at 63 °C is shown on the right



melting transition indicates that the ligands on silver nanoparticles are significantly more ordered than on gold, consistent with the qualitatively observed high solubility of the latter materials. Additionally, odd-even effects were observed, where the position of the most prominent phase transition shifts to higher temperatures for alkylthiols with an odd number of carbons in the chain. These temperatures are 138 °C and 140 °C for $n = 9$ and $n = 7$, respectively. Such odd-even effects have been observed previously for liquid crystals [27] and paraffins [28] where high temperature hexagonal ‘rotator’ phases of odd and even paraffins exhibit differences associated with interactions between chain ends. The odd-even effects are manifested in other properties, specifically wetting behavior, of 2D SAMS on gold due to the different surface projections of the methyl groups for odd and even-numbered carbon chains [29].

Polyfunctionalized nanoparticles containing a mixture of alkylthiols with different chain lengths show significantly different energetics of the phase transitions. It should be mentioned that recent studies have shown that some polyfunctionalized nanoparticles of gold and silver particles have an inhomogeneous distribution of ligands in their shell [30]. Studies to clarify this point on such particles are underway. In any event we do not think that the distribution of ligands affects the results discussed hereafter. Moreover, recent combined STM and IR studies [31] show that phase separation does not occur on the ligand shell of octanethiol/undecanethiol-coated gold nanoparticles. The position of the major phase transition decreases by up to 25 °C as compared to the transition temperature for their counterparts coated with a single type of ligand, ‘monoligand’-coated nanoparticles, (e.g. 128 °C for C_{12} , 109 °C for C_{12}/C_8 , see Table 3, sample 2 versus sample 8). The lower temperature phase transitions are not evident for the mixed-ligand coated particles; instead a gradual energy absorption profile is observed. The energetics of the major phase transition were determined and evaluated in terms of the moles of organic coating for comparisons amongst nanoparticle samples. Using elemental analysis, the percentage of ligand relative to silver is determined and the value of J/g can be converted to $J/mole\text{-organic}$. In this way, the contribution of the organic shell, which is assumed to be responsible for the major component of this phase transition, is isolated. Table 3 provides a summary of data for this transition, where the molar ratio of silver to thiol is indicated in each case for direct comparison. The following trends are clear from this Table 3. (1) There is a general decrease in ΔG with decreasing ligand length, as seen in samples 1–6. (2) The order-disorder transition free energy change decreases upon mixing of ligands in the nanoparticle shell, where a mixture of two ligands results in a total enthalpy change which is less than that of the weighted average of that for the particles coated with the

Table 3 Summary of phase transition energetics for various particle sizes and ligands

Sample	Ag:RSH molar ratio	Ligands (ratio)	Transition temperature (°C)	ΔH (kJ/mol organic)	ΔG (kJ/mol organic)
1	3:1	C_{18}	131	42.3	11.1
2	3:1	C_{12}	128	36.4	9.3
3	3:1	C_9	138	16.0	4.4
4	3:1	C_8	128	20.6	5.3
5	3:1	C_7	140	10.4	2.9
6	3:1	C_6	129	8.2	2.1
7	3:1	C_{18}/C_{12} (1:1)	120	20.5	5.0
8	3:1	C_{12}/C_8 (3:1)	109	16.3	3.6
9	3:1	C_{12}/C_7 (3:1)	111	12.3	2.8
10	3:1	$C_{12}/C_8/C_7$ (1:1:1)	107	9.4	2.0
11	9:1	C_8	128	13.7	3.5
12	6:1	C_6	129	5.5	1.4
13	6:5	C_6	129	10.9	2.8
14	3:2	C_{12}/C_8 (3:1)	109	21.6	4.7
15	3:2	C_{12}/C_7 (3:1)	117	20.7	4.9

Alkylthiol ligands are identified by the number of carbons in the chain. Silver:ligand molar ratio represents the initial ratio of reagents used (larger silver to thiol ratios give larger particles, see Table 1)

two ligands separately (i.e.#7 vs. #2, #9 vs. #5). (3) The size of the core does not affect the transition temperature, but the enthalpy change is altered (sample numbers 11–13).

The DSC data show that mixtures of ligands significantly reduce the melting energy of the superlattice assembly. For example, a mixture of octadecyl and dodecylthiol results in disordering energies comparable to those observed with monofunctional silver nanoparticles coated with octylthiol, a shorter ligand, alone. This has an extremely useful application where greater interparticle separations are required and solubility is important. Further polyfunctionalization results in an even larger increase in disorder. Indeed, a mixture of dodecylthiol, octylthiol, and heptylthiol ligands on silver particles results in the lowest superlattice melting enthalpy measured, which is comparable to that found for monofunctional hexylthiol-coated silver nanoparticles. These low melting energies are attributed to the fact that neighboring ligands that are of differing chain lengths will not retain the alkyl chain order. For example, in the case of dodecylthiol and octylthiol ligand mixtures, the last four carbons in the dodecylthiol chain will be free to rotate and form gauche conformations, as depicted in Fig. 3a. In keeping fully ordered domains from forming, the interdigitation, or space filling, of bundles on neighboring particles is impeded. Also, the melting

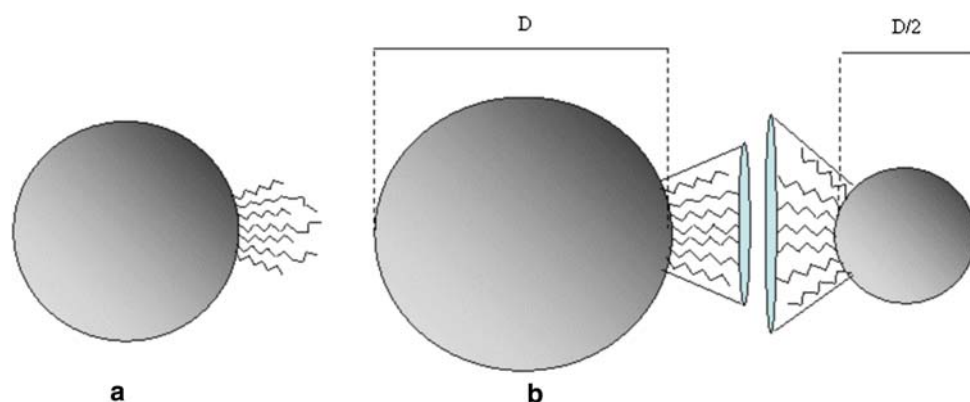


Fig. 3 Schematic illustration of a polyfunctionalized nanoparticle (left) with a small ligand domain shown. Note the disorder of the terminal methylenes and methyl group, resulting in an overall partially disordered shell. The surface curvature has significant effect

on the radial curvature of the ligands (right). Note the curvature of the ligand shell is larger for smaller particles, resulting in more defect/open sites for interdigitation with neighboring ligands

transition of these longer chains occurs at much lower temperatures and energies.

The effects of silver core size were also studied. Larger particles consistently showed lower melting enthalpies. A possible interpretation of these results lies in the surface curvature of the particles, as depicted in Fig. 3b. This figure was drawn so as to keep the spacing of the ligands at the particle surface nearly the same. Though the surface is actually faceted, the many defects and edge sites result in a roughly spherical shape. For larger particles, the ligands pack tighter with more ordered bundles with less free space that would allow for packing with the ligands of the neighboring particles. In the case of smaller particles, there are more defects and open spaces where bundles from neighboring ligands may pack.

A final alteration made to enhance solubility involves the addition of a terminal pendant group to promote favorable intermolecular interaction with the host material. For example, a carbazole moiety was attached to the ω position of an octylthiol chain (*N*-octylthiol carbazole), and nanoparticles whose coatings included this ligand displayed significant solubility in PVK.

The polysubstituted silver nanoparticles were found to be the most soluble and useful in the formation of nanocomposites for laser based metal microfabrication applications, as shown in Fig. 4. As discussed above, the relative ratios of different alkylthiol ligands for a sample of silver nanoparticles are controllable parameters. However, to establish that these particles were indeed coated with a ligand mixture versus a situation where the alkylthiols segregate according to length, resulting in samples that contain a mixture of monoligand-functionalized nanoparticles we used additional DSC measurements. As the melting of the alkyl chains on mono-ligand-coated nanoparticles occurs between 126 and 131 °C and mixtures of

ligands melt at lower temperatures (up to 25 °C lower), DSC can be a useful tool for discriminating between the two possible situations. Experiments were performed by placing a mixture of these two powders (dodecylthiol and octylthiol-coated silver nanoparticles) in the sample pan and subjecting this sample to three heating-cooling cycles. Upon mixing of solid samples of the two different coated nanoparticles in the sample pan, the expected behavior of a physical mixture of two nanoparticle species was observed with peaks at 126 and 131 °C (See Fig. 5). However, repetitive heating and cooling cycles resulted in a steady decrease in the energy change and temperature of the alkyl disordering phase transition, with the ultimate transition occurring at 108 °C (similar to that observed for samples 8 and 14, Table 1). This reveals that the silver-thiolate bond is quite labile at high temperatures, allowing for facile place exchange to occur, and indicates that the silver nanoparticles most likely contain a mixture of the various alkylthiolates. Additionally, this supports the conclusion that the polyfunctionalized nanoparticles discussed are indeed capped with shells containing mixtures of ligands, and are not simply a physical mixture of the monofunctionalized materials.

We observed that the free energy of the alkyl chain disordering could be correlated to nanoparticle solubility and dispersibility in polymer matrices. In order to further substantiate the solubility of the nanoparticles beyond qualitative observations, solubility measurements were carried out using optical density measurements to monitor the concentration of silver nanoparticle solutions. Noble metal nanoparticles typically display a surface plasmon resonance, which is characterized by high molar extinction coefficients, approaching $1 \times 10^9 \text{ L mol}^{-1} \text{ cm}^{-1}$ [32]. The molar extinction coefficient was first determined from dilute solutions of each sample of silver nanoparticles,

Fig. 4 Improvements in optical quality of PVK films containing similar silver nanoparticle loadings (1% by weight). By decreasing the ligand length, mixing ligands, adding functional carbazole groups to the ligand terminus for favorable host interactions, and increasing the particle core size, high quality films such as that shown on the right can be obtained

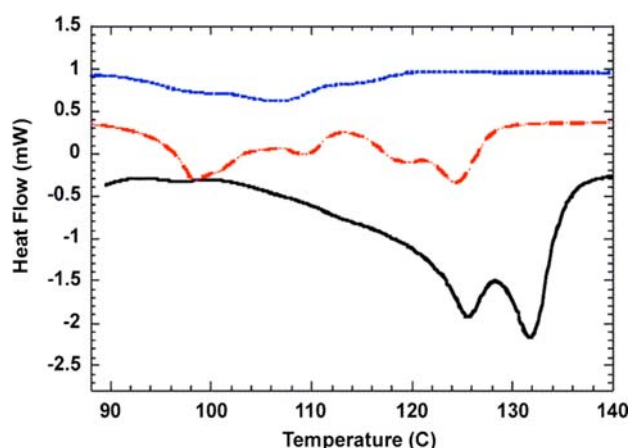
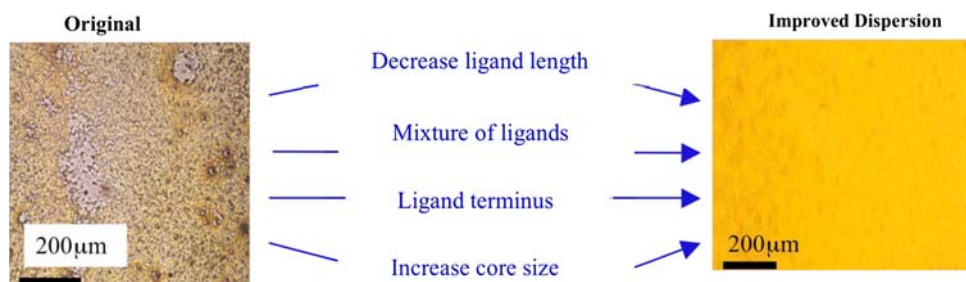


Fig. 5 DSC traces for mixtures of powders of monoligand-coated nanoparticles, cycled from 50 to 150 °C. Monofunctionalized silver nanoparticles prepared with octylthiol and dodecylthiol were used, showing individual phase transitions at 126 and 131 °C, respectively. In the initial cycle (solid black), separate disorder peaks were seen, corresponding to the monofunctionalized particles. After the second cycle (red dashed), new peaks develop at approximately 100 °C and 110 °C, while the two original peaks decrease in both temperature and energy. On the third heating cycle (blue dotted) the peaks merge at approximately 108 °C, the temperature at which the phase transition for silver nanoparticles prepared with mixtures of these two ligands occurs (see Table 3)

from which the concentration of saturated solutions was extracted. This allowed for the determination of the solubility, for which the results are shown in Table 4. From this data, the trend of increasing solubility with decreasing enthalpy change of superlattice melting is confirmed.

Finally, to establish the identity of the bulk product (as probed by DSC) and as opposed to the soluble portion (which is probed by the solubility studies) the silver nanoparticle samples were subjected to further purification in several cases, whereby the soluble portion was separated from the insoluble portion and each studied separately. It was often found that there was a significant amount of insoluble material present, even when suitable solvents are added, which necessitates filtering for further application. As expected, this insoluble portion is more significant for

Table 4 Saturation concentrations of ligand coated silver nanoparticles in hexane solutions and comparison to free energy change of superlattice melting as measured by DSC

Sample number	ΔG of alkyl melting (kJ/mol organic)	Concentration of saturated solution (g/L $\times 10^2$)
1	11.1	0.165
5	2.9	0.712
9	2.8	4.84
6	2.1	8.04
10	2.0	27.6

Sample numbers refer to the compositions in Table 3

the nanoparticle samples that display greater superlattice melting energy. Powder XRD of this insoluble portion showed no evidence of bulk silver metal, suggesting that the lack in solubility is the result of tightly entwined nanoparticle ligand shells and not bulk silver aggregates. The soluble portion yielded a crystalline, shiny gray/black material, while the insoluble portion was a matte black in all cases. The data in Table 5 show that both materials investigated (C_{12} thiol and C_{12}/C_8 thiol coated silver nanoparticles) show similar trends. Notably, all three fractions ('as-prepared', soluble, and insoluble) have nearly identical silver to organic ratios, suggesting that the final product is composed of the same material, essentially alkylthiol-coated silver nanoparticles. The separated fractions simply have varying degrees of solubility due to differences in the order of the ligands. The degree of insolubility is directly related to the energy change associated with the most prominent DSC transition, an important confirmation of our empirical relation between melting transition and solubility. TEM studies of the soluble portion show that the distance between the particles approaches that of one ligand length, indicating that the ligands are still substantially interdigitated on the TEM grid (Fig. 6).

Table 5 Elemental analyses and enthalpy changes for phase transitions (130 °C) of separated nanoparticle fractions prepared via one-phase and two-phase methods

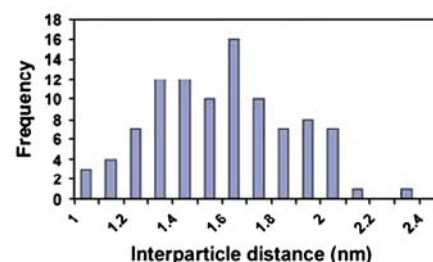
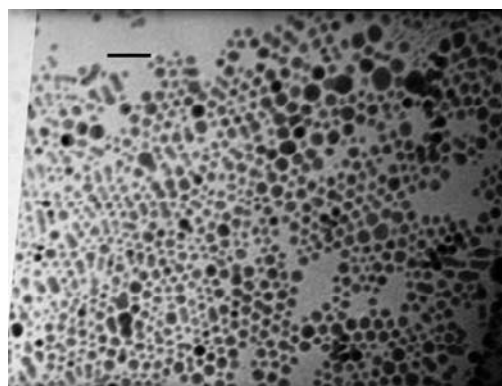
Fraction	Ligand length	%C	%Ag	$n_{\text{Ag}}/n_{\text{organic}}$	ΔH
Initial	C ₁₂	23.5	62.9	3.2	38.0
Insoluble	C ₁₂	24.5	62.9	3.2	46.4
Soluble	C ₁₂	23.8	62.9	3.2	25.4
Initial	C ₁₂ /C ₈	14.1	74.6	4.4	20.6
Insoluble	C ₁₂ /C ₈	14.3	73.9	4.2	31.3
Soluble	C ₁₂ /C ₈	13.7	71.5	3.8	9.7

The initial material is the raw product, the insoluble fraction is the remainder of the raw product after washing with hexane, and the soluble fraction is the isolated, hexane-soluble material. The ligand mixture used is 1:3 C₁₂/C₈

3 Conclusions

We have carried out DSC measurements on a series of alkylthiol-coated silver nanoparticles in order to develop an understanding of the ligand disordering processes. An effective structure-property relationship was found that correlates the nature of the ligands with the temperature and enthalpy change associated with the nanoparticle superlattice melting. Consequently, the solubility of silver nanoparticles in organic solvents was optimized in a rational manner, allowing for the preparation of high quality polymer composites containing these nanoparticles. It was found that silver nanoparticles with a lower energy of ligand disordering showed an increased solubility in organic solvents, and can afford nanoparticle/polymer composite films with an improved dispersion, high optical quality and homogeneity. In all cases, nanoparticle synthesis resulted in materials containing a portion that was soluble in nonpolar solvents. These soluble portions exhibited a smaller enthalpy change for the disordering transition in comparison to the bulk, insoluble portion, confirming that a direct relationship exists between the enthalpy change of the phase transition around 130 °C and the solubility of the nanoparticles. This understanding leads

Fig. 6 TEM image of dodecylthiol-capped silver nanoparticles and corresponding interparticle distances, which are approximately one all-trans ligand length. The length of an all-trans dodecylthiol ligand is approximately 1.6 nm (scale bar = 20 nm)



to a rational design criterion for silver nanoparticles with enhanced solubility for desired applications. Larger nanoparticles, nanoparticles with ligand mixtures, and those with shorter alkyl chains display significantly higher solubility due to the introduction of disorder within the ligand shell. These studies have provided insight to the factors that govern the nanoparticle assembly process, and have shown a reliable method for obtaining tunable solubility in silver nanoparticles for increased processibility, which is expected to be an important factor in their continuing use towards new applications.

4 Synthesis

The following were supplied by Aldrich: dichloromethane, hexane, silver nitrate (99.999%), hexylthiol, heptylthiol, octylthiol, nonylthiol, dodecylthiol, octadecylthiol and sodium borohydride (98%). Ethanol (200 proof) was supplied by Aaper, Shelbyville, KY. All reagents were used as received.

4.1 Synthesis of Alkylthiol-stabilized Metal Nanoparticles

Syntheses of silver nanoparticles *via* the so-called ‘one phase’ method employed ethanol as the solvent. To a solution of silver nitrate (0.340 g, 2.00 mmol) in ethanol (100 mL) at ~0 °C was added alkylthiol (either neat or, in the case of octadecylthiol, as a solution in 10 mL of ethanol). The amounts of alkylthiol (RSH; where R = *n*-alkyl chain with C6, C7, C8, C9, C12, C18) used varied from 2.00 mmol to 0.17 mmol. A light yellow/white cloudy solution resulted from addition of alkylthiol (indicating the formation of a silver thiolate) and the mixture was stirred for 1 h. To this solution was added a saturated solution of NaBH₄ in ethanol (6–7 mmol) dropwise from an addition funnel with vigorous stirring of the solution until a dark brown color was seen, after which the speed of addition was increased. The solution was stirred an additional 3 h

before refrigerating overnight to induce precipitation. A cannula was used to decant the ethanol to avoid disturbing the settled nanoparticles, which can easily be re-suspended. The final thick solution was filtered and the dark solid collected was washed copiously with ethanol, acetone (to remove excess alkylthiol) and water (to remove excess water soluble species). The material was washed with acetone again, dried for 24 h under vacuum and stored in powder form. $^1\text{H-NMR}$ analysis of the product revealed no excess alkylthiol to be present in the collected materials. Typical yields from this synthesis were *ca.* 250 mg. This method was successfully repeated on a scale of $\frac{1}{4}$ mmol to 4 mmol AgNO_3 . Silver nanoparticles containing mixtures of *n*-alkylthiols, and a mixture of *n*-octylthiol and carbazolethiol [17] were prepared in the same manner.

4.2 Purification

A fraction of the final product was usually found to be soluble in organic solvents (e.g. hexane, methylene chloride), whereas a fraction was not. To separate the soluble material, the crude product was washed with hexane until the washings were colorless. It was difficult to induce precipitation of nanoparticles from the hexane filtrate; for more efficient collection, the solution was concentrated to near dryness by rotary evaporation. A film was formed on the sides of the flask that could not be removed by scraping. Hexane (~ 5 mL) was used to rinse the sides and collect a concentrated solution on the bottom of the flask, which was evaporated under a stream of dinitrogen. The crystalline material was collected by addition of acetone, scraping, and filtration. Both ‘soluble’ and ‘insoluble’ fractions were analyzed.

4.3 Solubility Measurements

The solubility of the nanoparticles was determined via the optical density of the nanoparticle solutions. Dilute solutions of each nanoparticle of interest were made in hexane with known concentrations. From this, the extinction coefficient was found. The linearity of the plot also indicated solubility versus suspended particles. Then, saturated solutions were made by stirring for one day at 25°C . The solutions were filtered through a $0.02\ \mu\text{m}$ filter, and diluted appropriately to place them in the linear regime of a Beer’s Law plot. From this, the original concentration and hence the solubility of the saturated solutions was determined.

4.4 Characterization

Differential scanning calorimetry (DSC) and thermogravimetric analysis (TGA) were performed using a Shimadzu

DSC/TGA 50, which is connected to a personal computer via a Shimadzu TA 50 thermal analyzer, under a nitrogen-purged atmosphere, using aluminum pans. Scan speeds were $10^\circ\text{C}/\text{min}$. Gas chromatography-mass spectrometry (GC-MS) was performed using a JP 6890 gas chromatograph equipped with a mass selective detector HP 5973. Elemental analysis was performed either by Atlantic Microlab, Inc., Norcross, GA or by Desert Analytics Laboratory, Tucson, AZ. TEM was performed using a Hitachi 8100S (University of Arizona) or a JEOL 100CX II (Georgia Institute of Technology). The samples were cast on Si_3N_4 grids purchased from SPI, West Chester, PA, USA or on lacey carbon mesh grids (Ted Pella). Size analyses were conducted on at least 50 particles (although usually over 100 were selected) utilizing ImageJ or NIH image software. Optical measurements were obtained using a Hewlett Packard diode array spectrophotometer.

Acknowledgements Support of this work by the National Science Foundation NIRT program (DMR-0454533) and the Office of Naval Research (N00014-00-1-10633 and N00014-03-1-0793) is gratefully acknowledged.

References

1. Faraday M (1857) *Philos Trans R Soc* 147:145
2. Brust M, Walker M, Bethell D, Schiffrin D, Whyman R (1994) *J Chem Soc Chem Commun* 801
3. Brust M, Fink J, Bethell D, Schiffrin D, Kiely C (1995) *J Chem Soc Chem Commun* 1655
4. (a) Hostetler MJ, Templeton AC, Murray RW (1999) *Langmuir* 15:3782; (b) Templeton A, Hostetler M, Warmoth E, Chen S, Hartshorn C, Krishnamurthy V, Forbes M, Murray R (1998) *J Am Chem Soc* 120:4845
5. Heath JR, Knobler CM, Leff DV (1997) *J Phys Chem B* 101:189; Harfenist SA, Wang ZL, Alvarez MM, Vezmar I, Whetten RL (1996) *J Phys Chem* 100:13904
6. (a) Stoeva SI, Prasad B, Uma S, Stoimenov PK, Zaikovski V, Sorensen CM, Klabunde KJ (2003) *J Phys Chem B* 107:7441; (b) Martin JE, Wilcoxon JP, Odinek J, Provencio P (2000) *J Phys Chem B* 104:9475
7. Murray C, Kagan C, Bawendi M (2001) *Ann Rev Mater Res* 30:545
8. Badia A, Gao W, Singh S, Demers L, Cuccia L, Reven L (1996) *Langmuir* 12:1262
9. Badia A, Cuccia L, Demers L, Morin F, Lennox R (1997) *J Am Chem Soc* 119:2682
10. Hostetler M, Stokes J, Murray R (1996) *Langmuir* 12:3604
11. Wang Z, Harfenist S, Whetten R, Bentley J, Evans N (1998) *J Phys Chem B* 102:3068
12. Jana NR, Pal T (1999) *Langmuir* 15:3458
13. Wang JF, Gudixsen MS, Duan XF, Cui Y, Lieber CM (2001) *Science* 293:1455
14. (a) Nie S, Emory SR (1997) *Science* 275:1102; (b) Wenseleers W, Stellacci F, Meyer-Friedrichsen T, Mangel T, Bauer C, Pond S, Marder S, Perry J (2002) *J Phys Chem B* 106:6853
15. Bockstaller M, Kolb R, Thomas E (2001) *Adv Mat* 13:1783
16. Dirix Y, Bastiaansen C, Caseri W, Smith P (1999) *Adv Mat* 11:223

17. Stellacci F, Bauer C, Meyer-Friedrichsen T, Wenseleers W, Alain V, Kuebler S, Pond S, Zhang Y, Marder S, Perry J (2002) *Adv Mat* 14:194
18. Whetten RL, Shafiqullin MN, Khoury JT, Schaaff TG, Vezmar I, Alvarez MM, Wilkinson A (1999) *Acc Chem Res* 32:397
19. Kang S, Kim K (1998) *Langmuir* 14:226
20. Waters CA, Mills AJ, Johnson KA, Schiffrin DJ (2003) *Chem Comm* 540
21. Daniel M-C, Astruc D (2004) *Chem Rev* 104:293
22. Hostetler M, Wingate J, Zhong C, Harris J, Vachet R, Clark M, Londono J, Green S, Stokes J, Wignall G, Glish G, Porter M, Evans N, Murray R (1998) *Langmuir* 14:17
23. Stellacci F, Bauer CA, Meyer-Friedrichsen T, Wenseleers W, Marder SR, Perry JW (2003) *J Am Chem Soc* 125:328
24. Love JC, Estroff LA, Kriebel JK, Nuzzo RG, Whitesides GM (2005) *Chem Rev* 105:1103
25. Badia A, Singh S, Demers L, Cuccia L, Brown G, Lennox R (1996) *Chem-Eur J* 2:359
26. Badia A, Back R, Lennox RB (1994) *Angew Chem Int Ed Engl* 33:2332
27. Grupta VK, Abbott NL (1999) *Langmuir* 15:7213
28. Craievich A, Doucet J, Denicolo I (1985) *Phys Rev B* 32:4164
29. Lee S, Puck A, Graupe M, Colorado JR, Shon Y-S, Lee TR, Perry SS (2001) *Langmuir* 17:7364
30. (a) Jackson AM, Myerson JW, Stellacci F (2004) *Nat Mater* 3:330; (b) Jackson AM, Hu Y, Silva PJ, Stellacci F (2006) *J Am Chem Soc* 128:11135
31. Centrone A, Zerbi G, Stellacci F (2007) *Small* 3:814
32. Kelly KL, Coronado E, Zhao LL, Schatz GC (2003) *J Phys Chem B* 107:668